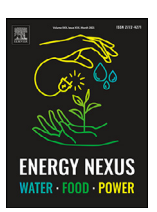


Contents lists available at ScienceDirect

Energy Nexus

journal homepage: www.elsevier.com/locate/nexus



Design of an integral terminal-based sliding mode controller for PV and BESS-based DC microgrids



T.K. Roy^{a,*}, M.A.H. Pramanik^b, S.K. Ghosh^c

- ^a Department of Electronics & Telecommunication Engineering, Rajshahi University of Engineering & Technology, Rajshahi, 6204, Bangladesh
- b Department of Electrical & Computer Engineering, Rajshahi University of Engineering & Technology, Rajshahi, 6204, Bangladesh
- ^c Department of Electrical & Electronic Engineering, Rajshahi University of Engineering & Technology, Rajshahi, 6204, Bangladesh

ARTICLE INFO

Kevwords:

Battery energy storage system DC microgrid Lyapunov control theory Renewable energy nexus Reachability analysis

ABSTRACT

Conventional power generation is undergoing a dramatic upheaval, and renewable-based microgrids are playing an important part in this energy sector revolution. An integral terminal sliding mode controller based on a double-power reaching law control strategy for solar photovoltaic and battery-based DC microgrid systems has been proposed in this paper for the energy-environment nexus. First, a thorough mathematical model of the DC microgrid's components is developed based on their electrical properties. The controller is therefore developed with the key goal of maintaining a consistent DC-bus voltage during the DC microgrid's transient and steady-state situations. The asymptotic stability of the DC microgrid is then proven using the Lyapunov control theory. Finally, the proposed controller's applicability is investigated using thorough analysis on both simulation and real-time platforms, as well as rigorous comparison studies with an existing sliding mode controller. For simulation studies, the MATLAB/Simulink platform is used, while the processor-in-loop validations of the proposed approach are performed on a Rasberry Pi 3B Quad-Core 64-bit Microprocessor Development Board.

1. Introduction

1.1. Background and motivation

Due to technological innovation and a growing population, fuel consumption for power generation has expanded dramatically to meet the needs of the energy nexus [1,2]. For power generation, fossil fuels, such as coal and petroleum are used, which has led to their rapid depletion and a variety of other ecological problems. Therefore, to meet the needs of economic and social development while reducing the emission of environment pollutant (e.g., CO, CO2, SO2, etc.) researchers have been encouraged to incorporate renewable energy sources (RESs), such as solar photovoltaic (SPV), wind, etc. with the existing power grid [3,4]. However, because of the high potential installation costs of RESs, it is always better to run them at high efficiency levels [5,6]. In this context, the formation of microgrids (MGs) is an efficient option for the high integration of RESs along with an energy storage system (ESS), and variable loads into current power networks [7-9]. For energy nexus, an MG provides numerous advantages, including high reliability, minimal losses, greater adaptability, and feasibility in terms of installation [10]. MGs can be classified as ACMGs or DCMGs based on the common-bus voltage. Due to their simple construction, DCMGs have acquired widespread adoption over the ACMGs [11]. In addition, controlling a DCMG is simpler than controlling an ACMG since there are no reactive power flow, frequency control harmonics, or grid synchronization difficulties [12,13].

The SPV unit cannot deliver consistent power due to the unpredictability of solar irradiation. Furthermore, a sudden shift in load demand could have a major impact on the DCMG's performance at the nexus of energy requirements [14,15]. In this case, power supply dependability to the load cannot be guaranteed since the DC-bus voltage will not be constant, even though a constant voltage is required to maintain power balance. As a result, one of the most significant challenges in maintaining power balance for energy nexus is maintaining a consistent DC voltage at the DC-bus while improving system stability and efficiency [16,17]. This issue may be rectified by connecting an energy storage system (ESS) to the DC-bus, which will provide power dependability by maintaining power balance inside the microgrid [18]. A DCMG's ESS needs to be controlled in a way that it will help to maintain the power balance within the system; that is, when there is insufficient power from RESs to meet the load demands, it will deliver power to the load; and when there is more than the total load demands, it will store the excess power [19]. This control goal may be realized by interfacing the ESS with a DC-DC bidirectional converter (DDBC), which will operate in the boost and buck modes depending on the condition of the DC-bus voltage [20,21]. On the other hand, a DDBC combined with a DC-DC boost converter (DBC) based DCMG is highly nonlinear and com-

* Corresponding author.

E-mail address: tkroy@ete.ruet.ac.bd (T.K. Roy).

Nomenclature

 P_{net} The net power of the microgrid (kW) P_{pv} The solar PV output power (kW) P_{BESS} The BESS output power (kW) P_{Load} The DC load power (kW) C_{dc} The DC-bus capacitor (μF) DC-bus voltage (V) V_{dc} The state of charge of a BESS (%) SoCMaximum state of charge of a BESS (%) SoC_{max} SoC_{\min} Minimum state of charge of a BESS (%)

 $\begin{array}{ll} I_{charge} & \text{Charging current of a BESS (A)} \\ I_{B} & \text{The current of a BESS (A)} \\ I_{discharge} & \text{Discharging current of a BESS (A)} \\ i_{I-m} & \text{Input current of the converter for a PV unit (A)} \end{array}$

 $i_{L_{pv}}$ Input current of the converter for a PV unit R_{pv} Converter's resistance for a PV unit Ω Converter's inductance for a PV unit Ω

 μ_{pv} Control input for the PV unit

 i_{opv} Output current of a converter for a PV unit (A) i_b Input current of the converter for a BESS (A)

 $\begin{array}{ll} \mu_b & \quad \text{Control input for the BESS unit} \\ R_b & \quad \text{Converter's resistance for a BESS } (\Omega) \\ L_b & \quad \text{Converter's inductance for a BESS } (\text{mH}) \end{array}$

 V_b Output voltage of the BESS (V)

 i_{ob} Output current of a converter for a BESS (A)

 S_{pv} Sliding surface for a PV unit e_{pv} Error signal for a PV unit (A)

 $i_{Lpv(ref)}^{\prime}$ Reference current of the converter for a PV unit (A)

 t_r The reaching time (s) γ_{pv} A positive design constant

 $sgn(S_{pv})$ Signum function

lpha Gain parameter of the controller eta Gain parameter of the controller W_{pv} Control lyapunov function K_{1b} Gain parameter of the controller K_{2b} Gain parameter of the controller K_{3b} Gain parameter of the controller

 $i_{b(ref)}$ Reference current of the converter for a BESS (A)

 $\begin{array}{ll} K_b & \text{Gain parameter of the controller} \\ V_{mp} & \text{Solar PV voltage at MPPT (V)} \\ i_{mp} & \text{Solar PV current at MPPT (A)} \\ Q_{bat} & \text{Rated capacity of the BESS (Ah)} \end{array}$

plicated. Therefore, to maintain the balance of power between supply and load, the coordination of different sources, such as wind and SPV, as well as their regulation, is a vital aspect of an MG [22,23]. Moreover, an effective control approach to manage the DC bus voltage and guarantee power balance is critical for the DCMG's regular operation. To achieve such objectives, the main focus of this study is on presenting an appropriate DCMG architecture as well as an effective control and energy management strategy for the nexus of energy requirements.

1.2. Relevant literature

In order to optimize the usage of RESs, researchers recently presented alternative topologies, control methodologies, and energy management approaches for DCMGs energy nexus. In [24], a multilayer converter based on pulse width modulation (PWM) is proposed for control-

ling the charging/ discharging current activities of a BESS in DCMGs. Although this converter accomplishes the needed control aim, its utility in terms of implementation is limited due to its layered nature. To overcome this constraint, [25] uses a dual active bridge (DAB)-based converter to connect the DC-bus to a BESS. Despite its ease of construction, it has some drawbacks in DCMG applications. In [26], an internet of thing (IoT)-based energy-food-water nexus is proposed to handle a variety of complicated problems. A neighboring microgrid including an urban agriculture plant for the food-water-energy nexus is proposed in [27]. In [28], a microgrid is proposed for the water-energy nexus as a single system that is very cost-effective and may be used in smart buildings, cities, communities, and villages. Another islanded microgrid for the water-energy nexus to maximize energy efficiency is proposed in [29]. However, the control approaches are not clear in the abovementioned papers. To avoid this limitation, a PID controller for a solarbattery based DCMG in the energy nexus framework is proposed in [14].

Droop control, as detailed in [30,31], is a successful control strategy for managing DC-bus voltage in MGs while ensuring proper load current sharing. The major weakness of a droop controller is that voltage drop effects across the line impedance decrease the precision of load current sharing. Ref. [32] offers a gain-scheduling controller based on fuzzy logic that enables good DC-bus voltage management and optimal power balancing in solar-energy nexus for DCMGs to overcome this constraint. Ref. [33] presents another PI-based fuzzy logic controller for managing DC-bus voltage and smoothing power flow between generators and loads in an islanded DCMG for the solar energy nexus. A fuzzy logic controller's drawback is that system dynamics might not have been adequately represented since this controller's design process is frequently devoid of dynamical models. Furthermore, the controllers examined so far have been based on linearized models, which prevents them from delivering the appropriate control performance when the operating point varies [33]. Owing to several power electronics converters' inclusion, the DCMG is an intrinsically complex and nonlinear system. As a result, nonlinear controllers have gained increased attention to guarantee stable operation in a wide range of operating environments.

The model predictive controller (MPC) is a well-known digital nonlinear controller that optimizes the cost function to deliver the converter control output. A nonlinear MPC is presented in [34] to reduce the impact of pulse load in a DCMG for the solar energy-nexus. Ref. [35] suggests another MPC approach for maintaining the stability of a RES based DCMG for the energy nexus. However, the value of this control strategy is restricted owing to the requirement of lengthy and useless computations. A nonlinear feedback linearization control (FBLC) method, which has been successfully used in DCMG applications due to its canceling capabilities, can be used to solve this constraint. A nonlinear FBLC method is provided in [36] for adjusting DC-bus voltage while preserving power balance within the DCMG. In addition, another adaptive FBLC is provided in [37], in which previously unknown system characteristics are predicted using adaptation rules while improving power-sharing capabilities inside the MG. Although the above control strategy can enhance DC-bus voltage regulation, the targeted control goal depends on the particular system components. In practice, however, determining exact system parameter information is difficult since system parameters can be swiftly adjusted with the change of an operational point. Furthermore, this control strategy eliminates some beneficial nonlinear elements on occasion, which can help to increase the system's transient stability. To escape the limitations of FBLC schemes, the nonlinear backstepping control (BSC) scheme is a useful control approach that can improve the system's transient reactions even when the specific system parameters are unknown [38].

A nonlinear BSC is introduced in [39,40] for studying the dynamic stability of hybrid DCMGs under various operating conditions, with the SPV unit serving as the main power supply. The simulation results demonstrate that good voltage management and power balance are achieved. In [41,42] an adaptive BSC is described to enhance DC-bus

voltage while guaranteeing power balance when there are model uncertainties. Although the control techniques presented in [39–42], may achieve the required control aim, the complexity of computing a derivative for every virtual factor causes considerable problems in the actual implementation, especially when the system order is greater. Furthermore, the effective performance of this control approach is contingent on the correct adjustment of the user-defined gain levels, complicating matters further.

According to Mi et al. [43], Ghosh et al. [44], nonlinear sliding mode control (SMC) is a possible way to get over BSC and FBLC limitations. A nonlinear SMC for DBCs is proposed in [45,46] to change the DCbus voltage by managing the bidirectional power flow between the MG components and the DC-bus. However, since they are not resilient to system uncertainties, these controllers require exact circuit parameters. As a result, an adaptive SMC has been proposed in [47,48] to increase robustness against parametric uncertainty. However, the SMC is divided into two sections, according to the literature: the reaching rule and the sliding surface. The reaching law aids system states in reaching the desired sliding surface, but it is challenging to maintain zero error on the sliding surface. The system states are always traveling on both sides of the sliding surface, causing the system to chatter. As a result, in the SMC, reducing chatter is critical. The design of the reaching law is critical in the SMC since it is directly tied to the system states reaching the sliding surface. As a result, several strategies for resolving the chattering problem have been proposed in the present literature, including super-twisting SMC [49], nonsingular fast terminal SMC [50], reaching law-based method [51], and others. On the other hand, the reaching law-based strategy, which focuses on the reaching phase, could be able to handle the chattering issue. To the best of the author's knowledge, the integral terminal SMC technique based on the double power reaching law is not employed to manage the DC-bus voltage in DCMG applications.

1.3. Contributions

To solve the aforementioned concerns with existing nonlinear control approaches in DCMG applications, this work proposes a nonlinear integral terminal SMC (ITSMC) with a double power reaching law (DPRL). To assist with the proposed controller design, a proper dynamical model is developed for each DCMG component. The proposed control method is then applied to each component to obtain the required control signal. The stability of the DCMG with the suggested control strategy is demonstrated using the Lyapunov control theorem. The suggested controller's main aim is to manage the DC-bus voltage while modulating the power flow between the generator and the load under various operating situations. As a result, the following are the primary contributions of this paper:

- A modified ITSMC based on a DPRL is proposed for a DCMG. This approach not only eliminates chattering, but it also increases transient stability.
- Because of the application of the DPRL, the suggested controller easily addresses the unexpected chattering problem that occurs in the existing control scheme.
- An integral terminal term is considered in the proposed control approach to increase convergence time and decrease steady-state tracking error.
- To illustrate the effectiveness of the proposed controller, simulation and real-time processor-in-loop (PIL) validations are performed.
- The suggested controller has excellent transient stability performance during operating point changes such as dramatic shifts in load demands, solar irradiance fluctuations, and so on.

To confirm the aforementioned contributions, the proposed controller's performance will be evaluated using various operating scenarios and compared to that of an existing SMC approach.

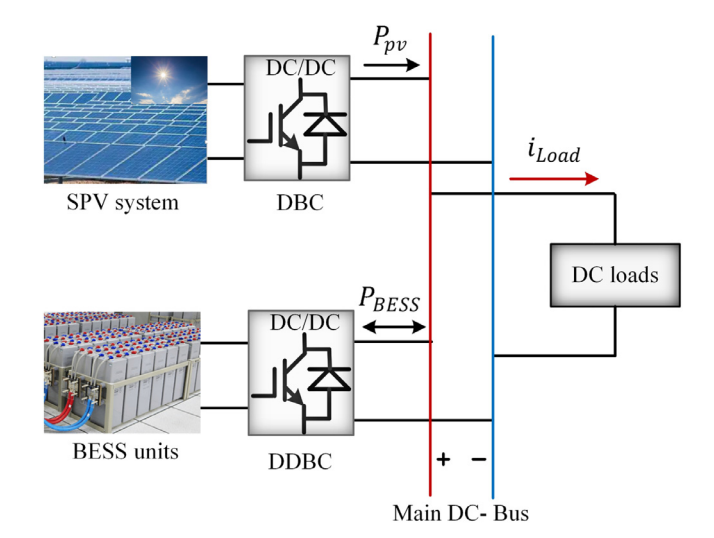


Fig. 1. Detailed structure of a PV dominated islanded DC microgrid.

2. Microgrid configuration and operating modes

This section explains the layout and operational modes of the proposed DCMG.

2.1. Configuration of the DCMG

Fig. 1 depicts the suggested RESs-based DCMG configuration. It is made up of an SPV unit, a BESS, and DC loads. Except for DC loads, all MG components are linked to the common DC-bus via their respective converters in this setup. It is worth noting that the SPV unit is the major power source in this configuration. Such systems are installed in this field for electrification in the rural areas where the main power grid is not available. Solar PV and battery-based DCMG systems are deployed to provide electricity in most rural regions, particularly in developing countries, such as Bangladesh. As the SPV's terminal voltage is too low concerning the MG's DC-bus voltage, it is interfaced with the DBC. A DBC is regarded as a dependable and promising technology for connecting an SPV's main power supply to the DCMG's DC-bus. The output power of the SPV should be sufficient to meet all load demands. However, if the SPV power cannot satisfy the load demand, additionally includes a BESS which provides the difference between generation and demand. Furthermore, if the SPV's output power is greater than the load demand, the BESS will store additional power to keep the network balanced.

2.2. Energy management unit and operational modes

As stated previously, maintaining power balance in DCMGs is a complicated matter since the output power of SPV units and the power required by loads are very unpredictable, resulting in a power mismatch and instability of the DC-bus voltage. Under this situation, an energy management unit (EMU) is responsible for coordinating and controlling all operations in the DCMG system. The EMU generates reference signals for each microgrid component based on the available measured input power in the DCMG system. To do that the net power equation can be written as follows:

$$P_{net} = P_{pv} \pm P_{BESS} - P_{Load} \tag{1}$$

where P_{net} is the net power, P_{pv} is the SPV output power, P_{BESS} is the BESS output power, which is positive while discharging and negative when charging, and P_{Load} is the power used by DC loads. It is often recognized that maintaining power balance in DCMG necessitates a constant DC-bus voltage. As a result, the DC-bus voltage dynamic can be

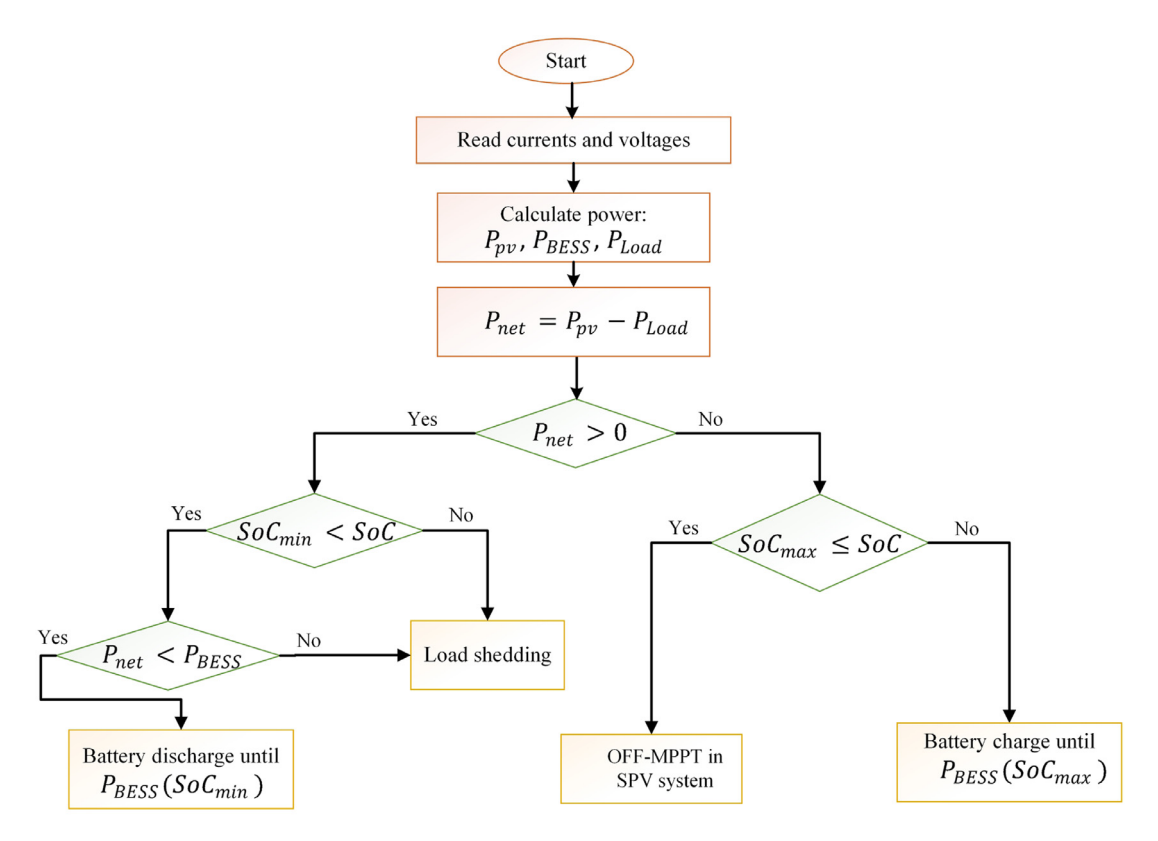


Fig. 2. The proposed energy measurement unit (EMU).

expressed as follows, depending on the net power:

$$C_{dc}V_{dc}\frac{dV_{dc}}{dt} = P_{net}$$
 (2)

where C_{dc} stands for the DC-bus capacitor. A constant DC-bus voltage implies a balanced power flow in DCMGs, as shown by Eq. (2). In contrast, an increase or fall in DC-bus voltage indicates a power excess or shortfall. The proposed controller in this work will be designed to maintain a constant DC-bus voltage by controlling the BESS's power flow while preserving the BESS's state of charge (SoC) in a safe operating condition. The flow chart of the proposed EMU is shown in Fig. 2. According to this EMU, this paper evaluates four main operating modes to maintain the power balance, which are discussed in more detail below:

Mode 1(Battery charging): In this state, the produced power of the SPV exceeds the whole load required. As a result, depending on the level of charge of the battery, excess power will be stored in the BESS through the DDBC's buck mode. In this mode, the DDBC controller's control operation for the BESS can be conditioned as follows:

if
$$(P_{net} > 0 \text{ and } SoC < SoC_{max})$$

then $(I_{charge} = -I_B)$ else $(I_{charge} = 0)$

As a result, the net power equation will be used in this scenario as follows:

$$P_{net} = P_{pv} - P_{BESS} - P_{Load} \tag{3}$$

Mode 2(Battery discharging): When the SPV output power is less than the entire load demand, this mode is activated. If the battery SoC is greater than the minimum SoC threshold and the difference between the SPV output power and total load demands in this mode is less than the rated battery power, the BESS will supply this shortfall power. As a result, the DDBC controller's control operation for the BESS may be conditioned as follows:

$$\begin{split} &\text{if } (P_{pv} < P_{Load} \text{ and } SoC > SoC_{\min}) \\ &\text{then } (I_{discharge} = I_B) \text{ else } (I_{discharge} = 0) \\ &\text{end} \end{split}$$

The net power equation will be used in this instance as follows:

$$P_{net} = P_{pv} + P_{BESS} - P_{Load} \tag{4}$$

Mode 3 (Turn off of the MPPT mode): In this mode, the BESS will be unable to absorb any power from the DC-bus as the battery's SoC satisfies the condition of $SoC > SoC_{\max}$. As a result, the DC-bus voltage will start to increase, making the DCMG unstable. To counteract this effect, the MPPT mode of the SPV unit is turned off, and the current duty ratio is kept constant. In this mode, the net power equation will be as follows:

$$P_{net} = P_{pv} - P_{Load} \tag{5}$$

Mode 4 (Load shedding): This mode will be activated if the SPV output power is less than the entire load demand and the battery hits the lower threshold of the *SoC* limit. Under this condition, load shedding will be initiated and DCMG will be forced to operate under Mode I.

Control laws must be developed using mathematical modeling of the MG components. These models are described in detail in the following section.

3. Each DCMG component's modeling

Each DCMG component is modeled separately in this section based on its unique features and requirements, which are in-depth described in the following subsections.

3.1. Model of DBCs

Fig. 3 displays the SPV system configuration, which includes a PV array and a DBC. The SPV system is connected to the DC-bus through a DBC and may function in MPPT and OFF-MPPT modes depending on the battery *SoC*. Now using Kirchhoff's laws, the dynamical model of an SPV unit can be described as follows:

$$\frac{di_{L_{pv}}}{dt} = \frac{1}{L_{L_{pv}}} [-R_{pv}i_{L_{pv}} - (1 - \mu_{pv})V_{dc} + V_{pv}]
\frac{dV_{dc}}{dt} = \frac{1}{C_{dc}} [(1 - \mu_{pv})i_{L_{pv}} - i_{opv}]$$
(6)

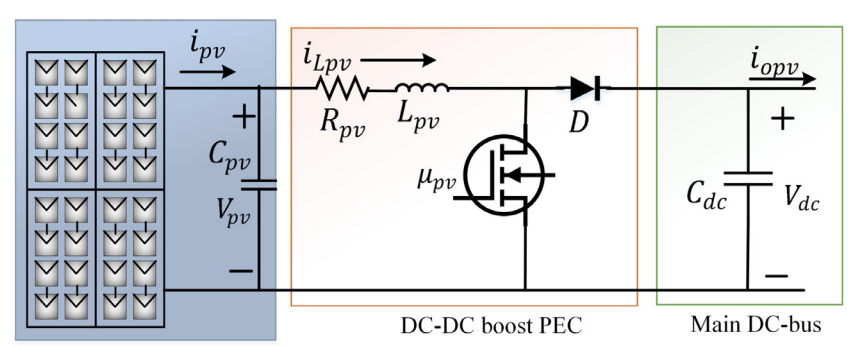


Fig. 3. An equivalent circuit configuration of a solar PV unit with a DBC.

Solar PV generation system

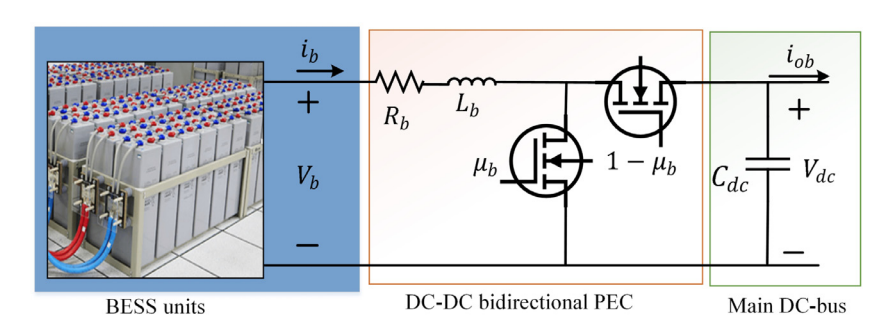


Fig. 4. An equivalent circuit configuration of the BESS with a DDRC

where V_{pv} , i_{Lpv} , C_{dc} , i_{opv} , and u_{pv} are used to represent the solar PV unit's output voltage, the internal inductance's L_{pv} current, and capacitance of the DC-bus, load current, and control signal, respectively.

3.2. Model of DDBCs

Because of the unpredictability of solar energy, BESS is employed to maintain a power balance in the DCMG. As indicated in Fig. 4, the BESS is linked to the DC-bus through a DDBC. From Fig. 4, the dynamical model may now be expressed as:

$$\frac{di_b}{dt} = \frac{1}{L_b} [V_b - R_b i_b - \mu_b V_{dc})
\frac{dV_{dc}}{dt} = \frac{1}{C_{dc}} (\mu_b i_b - i_{ob})$$
(7)

where i_b , V_b , L_b , R_b , i_{ob} , and μ_b indicate the BESS output current, BESS terminal voltage, converter inductance, internal resistance of the inductor, load current, and switching control signal, respectively.

To ensure the DCMG's smooth and efficient operation, effective control mechanisms must be established. To get the control law in this study, a nonlinear ITSMC technique based on a DPRL will be applied to each component of the MG, as presented in the next section.

4. Design of the proposed controller

A DCMG, as previously noted, is inherently an extremely nonlinear system. Furthermore, due to fluctuating load demands and solar irradiation, the operating point varies significantly in real-world applications. The nonlinear ITSMC will be built in this section to ensure the stability of the DCMG by applying the control signal to each component of the DCMG. The proposed controller design process is shown in the following sections.

4.1. Controller design for the SPV unit with a DBC

This section covers in detail the architecture of an ITSMC for the SPV unit to get the desired result. It is widely assumed that the design of any SMC requires two phases. In order to achieve the appropriate stability and dynamic performance, the sliding surface first needs to be properly chosen. Second, the reaching phase must be regulated using

an appropriate reaching rule such that the reaching time is minimized while chattering is kept to a minimum.

The following condition needs to be satisfied to design the proposed ITSMC using a DPRL:

$$S_{pv}\dot{S}_{pv} \le 0 \tag{8}$$

where S_{pv} is the sliding surface. According to the control objective, the tracking error (e_{pv}) for the inductor current is defined as:

$$e_{pv} = i_{Lpv} - i_{Lpv(ref)} \tag{9}$$

where $i_{Lpv(ref)} = K(V_{dc} - V_{dc(ref)})$ represents the reference current for inductor, while K is the proportional gain constant. Equation (6) can be used to characterize the tracking error dynamic and it can be written as follows:

$$\dot{e}_{pv} = N + \mu_{pv} M \tag{10}$$

where
$$M = \frac{V_{dc}}{L_{Lpv}} + K \frac{i_{Lpv}}{C_{dc}}$$
 and $N = \frac{1}{L_{Lpv}} [-R_{pv}i_{Lpv} - V_{dc} + V_{pv}] - K \frac{1}{C_{dc}} (i_{Lpv} - i_{opv})$. As previously mentioned, the first stage in the design of an SMC is always the choice of a sliding surface in terms of tracking errors. Therefore, an integral terminal sliding surface is defined as follows:

$$S_{pv} = e_{pv} + K_1 \int (\frac{\vartheta}{2} e_{pv} + \frac{\rho}{2\epsilon} e_{pv}^{\epsilon}) dt$$
 (11)

where ϑ , $\rho > 0$ and $0 < \varepsilon < 1$ where K_1 is a positive design constant and the right value of K_1 is always important in obtaining the required tracking performance. It is important to note that it is always preferable to get rid of chattering and successfully maximize finite convergence in order to improve overall performance. To accomplish this control purpose, the control law u_{pv} can be developed using a constant rate reaching law, as illustrated in [52], which fulfills $S_{pv}\dot{S}_{pv} \leq 0$ and it can be written as:

$$\dot{S}_{pv} = -\eta_{pv} sgn(S_{pv}) \tag{12}$$

where η_{pv} is a positive design constant. From Eq. (12), it can be seen that the degree of chattering may be seen to be directly regulated by η_{pv} . As a result, the following conundrum arises: to have a shorter reaching time, more robustness, and better tracking performance, η_{pv} must be increased. However, this will make the control input chatter more aggressively. The connection between the reaching time and the chattering

Table 1System and control parameters of the proposed DC microgrids.

Solar PV unit			
Parameters	Values		
Voltage at MPPT, V_{mp}	31 V		
Current at MPPT, i_{mp}	8.06 A		
Converter's resistance, R_{pv}	$0.05~\Omega$		
Converter's inductance, L_{pv}	0.352 mH		
Solar PV unit's input capacitance	$2200~\mu F$		
Parameter of the BESS (Lithium Ion Battery)			
Nominal voltage of the BESS, V_b	72 V		
Rated capacity, Q_{bat}	150 Ah		
Converter's resistance, R_b	$0.053~\Omega$		
Converter's inductance, L_b	0.3 mH		
Parameter of the DC microgrid			
DC bus nominal voltage, V_{dc}	120 V		
DC bus capacitance, C_{dc}	$300 \mu F$		
Control parameters for the solar PV unit			
$\eta_{1pv},\eta_{2pv},K_1$	250, 450, 100		
lpha,eta	1.5, 0.9		
Control parameters for the BESS			
K_{1b}, K_{2b}, K_{3b}	200, 250, 150		
lpha,eta	1.5, 0.85		

level should be abolished to address this conundrum. This difficulty is addressed by the exponential reaching law, which is discussed in the next section. At this point, integration of Eq. (12) with respect to time will yield the reaching time t_r for e_{pv} , which can be written as follows:

$$t_{r-e_{pv}} = \frac{S_{pv}(0)}{\eta_{pv}} \tag{13}$$

where $S_{pv}(0)$ is the initial value of $S_{pv}(t)$. Equation (13) shows that the reaching time is inversely related to η_{pv} . The reaching time will be shorter if the value of η_{pv} is larger, but the chattering level will be higher. Choosing an appropriate value of η_{pv} would necessitate a trade-off between reaching time and chattering level. Several investigations have been done to minimize chattering by revising the reaching law. According to ref. [47], combining a constant-proportional and a power-rate reaching rule is a good idea. The proportional plus constant rate switching law looks like this:

$$\dot{S}_{pv} = -\gamma_{pv} S_{pv} - \eta_{pv} sgn(S_{pv}) \tag{14}$$

The following Eq. (15) can be written, by integrating both sides of Eq. (14) between zero and t_{reach}

$$\int_{S_{pv}(0)}^{S_{pv}(t_{reach})} \frac{dS_{pv}}{\gamma_{pv}S_{pv} + \eta_{pv}sgn(S_{pv})} = -\int_{0}^{t_{reach}} dt$$
 (15)

The reaching time, when $S_{nv} \ge 0$, can be obtained as:

$$t_{reach} = \frac{1}{\gamma_{pv}} ln(1 + \frac{\gamma_{pv} S_{pv}(0)}{\eta_{pv}})$$
 (16)

Again, the reaching time, when $S_{pv} \le 0$, can be obtained as:

$$t_{reach} = \frac{1}{\gamma_{pv}} ln(1 - \frac{\gamma_{pv} S_{pv}(0)}{\eta_{pv}})$$
 (17)

As a result, the reaching time under all situations may be easily expressed as:

$$t_{reach} = \frac{1}{\gamma_{pv}} ln(1 + \frac{\gamma_{pv} |S_{pv}(0)|}{\eta_{pv}})$$
 (18)

Despite the fact that the reaching time is significantly less than the CRRL reaching time, Eq. (14) demonstrates that the reaching law is unchangeable. To address this limitation, an adjustable reaching law is used to increase system resilience while decreasing chattering and rapidly reaching the sliding surface:

$$\dot{S}_{pv} = -\eta_{1pv} |S_{pv}|^{\alpha} sgn(S_{pv}) - \eta_{2pv} |S_{pv}|^{\beta} sgn(S_{pv})$$
(19)

where $\eta_{1pv} > 0$, $\eta_{2pv} > 0$, $\alpha > 1$, and $0 < \beta < 1$. When the system state is not close to the sliding surface, i.e., $|S_{pv}| > 1$, the first term in the reaching law will play an important role, while when the system state

is near to the sliding surface, i.e., $|S_{pv}| < 1$, the second term will play a significant role. As a result, the DPRL ensures a high reaching speed, and the system has exceptional transient and dynamic properties during the whole reaching operation. The dynamic of the sliding surface is now expressed as:

$$\dot{S}_{pv} = \dot{e}_{pv} + K_1 \left(\frac{\theta}{2} e_{pv} + \frac{\rho}{2\epsilon} e_{pv}^{\epsilon} \right) \tag{20}$$

Substituting Eq. (19) into Eq. (20), it will yield:

$$\begin{split} &-\eta_{1pv}|S_{pv}|^{\alpha}sgn(S_{pv})-\eta_{2pv}|S_{pv}|^{\beta}sgn(S_{pv}) &= \dot{e}_{pv} \\ &+K_{1}(\frac{\vartheta}{2}e_{pv}+\frac{\rho}{2e}e_{pv}^{\beta}) \end{split} \tag{21}$$

The substitution of \dot{e}_{nv} from Eq. (10) into Eq. (21) will yield:

$$-\eta_{1pv} |S_{pv}|^{\alpha} sgn(S_{pv}) - \eta_{2pv} |S_{pv}|^{\beta} sgn(S_{pv}) = N + \mu_{pv} M$$

$$+ K_1 (\frac{\vartheta}{2} e_{pv} + \frac{\rho}{2e} e_{pv}^{\epsilon})$$
(22)

The following control law can be chosen from Eq. (22)

$$\mu_{pv} = -\frac{1}{M} \left[K_1(\frac{\theta}{2} e_{pv} + \frac{\rho}{2\epsilon} e_{pv}^{\epsilon}) + \eta_{1pv} |S_{pv}|^{\alpha} sgn(S_{pv}) + \eta_{2pv} |S_{pv}|^{\beta} sgn(S_{pv}) \right]$$
(23)

At this stage, the stability of the DBC is investigated. The following control Lyapunov function is used to do this:

$$W_{pv} = \frac{1}{2} S_{pv}^2 \tag{24}$$

The derivative of Eq. (24) by utilizing Eq. (19) is represented as follows:

$$\dot{W}_{pv} = -\eta_{1pv} |S_{pv}|^{\alpha} sgn(S_{pv}) - \eta_{2pv} |S_{pv}|^{\beta} sgn(S_{pv})$$
(25)

with $|S_{pv}| = S_{pv} sgn(S_{pv})$. Since \dot{W}_{pv} is negative semi-definite for $|S_{pv}| = 0$ or negative definite for $|S_{pv}| \neq 0$, the DBC that is connected to an SPV system is stable. In the next subsection, the proposed design technique for the DDBC is provided.

4.2. Proposed controller design for the BESS with a DDBC

The BESS's DDBC uses the same controller design methodology as described the earlier subsection. Thus, to minimize reiteration, the whole design technique is not provided in this paragraph. Thus, the following control law is obtained using the same approach as described above:

$$\mu_b = \frac{1}{M_{1b}} [N_{1b} + K_{3b} (\frac{\theta}{2} e_b + \frac{\rho}{2^c} e_b^c) + K_{1b} |S_b|^{\alpha} sgn(S_b) + K_{2b} |S_b|^{\beta} sgn(S_b)]$$
(26)

where K_{1b} , K_{2b} , and K_{3b} , are positive constant parameters, $e_b=i_b-i_{b(ref)}$, $i_{b(ref)}$ is the reference value of i_b which is obtained as $i_{b(ref)}=K_b(V_{dc}-V_{dc(ref)})$ with a proportional gain k_b , $N_{1b}=\frac{1}{L_b}(V_b-R_bi_b)-\frac{K_b}{C_{dc}}i_{ob}$, $M_{1b}=\frac{K_b}{C_{dc}}i_b-\frac{V_{dc}}{L_b}$.

4.3. Prove of reachability

In this part, the finite time t is calculated with two cases such as when |S| > 1 and when |S| < 1 by taking nonzero initial state S(0).

When |S| > 1, the second term in reaching law, as represented by Eq. (19)), can be omitted, and the law is reached then

$$\dot{S}(t)_1 = -K_1 |S(t_1)|^{\alpha} sgn(S(t_1))$$
(27)

Equation (27) could be rewritten as follows after some mathematical tinkering:

$$\int d_{t1} = -\frac{1}{K_1} |S(t_1)|^{-\alpha} d(S(t_1))$$
 (28)

Thus, the required time t_1 from Eq. (28) is calculated as follows:

$$t_1 = \frac{1}{K_1(\alpha - 1)} |S(t_1)|^{1 - \alpha} \tag{29}$$

Again, when |S| < 1, the first term in reaching law as represent by Eq. (19) can be omitted, and the needed time t_2 can be computed as follows:

$$t_2 = \frac{1}{K_2(\beta - 1)} |S(t_2)|^{1 - \beta} \tag{30}$$

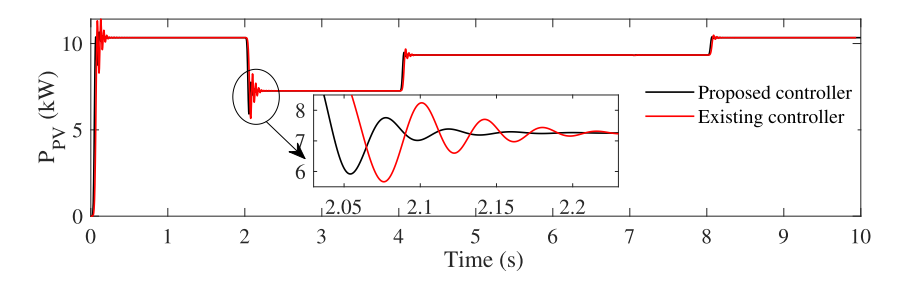


Fig. 5. Solar PV power response in the DC microgrid.

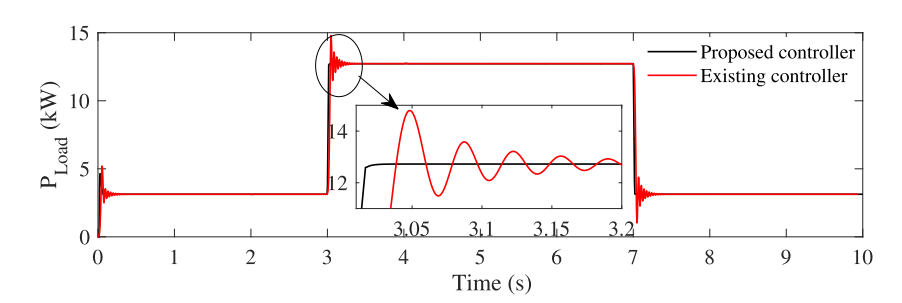


Fig. 6. Load power response in the DC microgrid.

At this point, the total convergence at a finite time can be stated by combining Eqs. (29) and (30) as:

$$t = t_1 + t_2 = \frac{1}{K_1(\alpha - 1)} |S(t_1)|^{1 - \alpha} + \frac{1}{K_2(\beta - 1)} |S(t_2)|^{1 - \beta}$$
(31)

Using the proposed controller, the tracking error will converge to zero in a finite period, according to Eq. (31). Moreover, it can be seen that DPRL enhances the sliding surface's reaching speed while maintaining the same gain K_1 and K_2 (i.e., the same chattering level). In addition, the gain K_1 and K_2 required for the reaching law of Eq. (19) is less than the η_{pv} required for Eq. (31) for the same reaching (13). As a result, the proposed approach minimizes chattering for the same reaching speed, which is a significant advantage over the usual reaching law. The next section includes simulation studies that demonstrate the usefulness of the controller in a DCMG.

5. Results and discussion

The proposed strategy is simulated in both MATLAB/Simulink and real-time PIL platforms to demonstrate the validity and usefulness of the designed control approach. The specifications and configuration of the MG used in the simulations are shown in Table 1. The simulation's goal is to assure the DCMG's steady operation by maintaining a constant DC bus voltage. The switching frequency of each converter is set at 5 kHz during the simulation, with a sampling frequency of 100 kHz. The developed, DPRL-based ITSMC controls the SPV unit and BESS. During MG operation, the battery will give appropriate power to the DC-bus to fulfill load demand when power is scarce and absorb excess power from the DC-bus when access power is available. To begin the simulation, turn on the SPV unit first to create the DC-link voltage, followed by the BESS and loads. Several operating situations are simulated, to validate the SPV and BESS performance in managing the DC-bus voltage while powering loads and maintaining the power balance. These scenarios are shown in the diagrams below. The proposed nonlinear controller's efficacy is also compared to that of an existing SMC, as investigated in [49].

5.1. Simulation results

Under typical atmospheric conditions, the PV output power during the first interval, i.e. from t=0 s to t=2 s, is 10.34 kW, whereas the total load demand is 3.013 kW. As the total generation exceeds the total load demand, the excess power would be stored in the BESS using the DDBC's buck mode, depending on the battery's SoC. All of these responses could

Table 2Quantitative evaluation for the SPV.

Transient time	Settling time (s)		Overshoot %	
(s)	Proposed	Existing	Proposed	Existing
2	0.208	0.359	6.896	13.489
4	0.151	0.234	1.532	3.706
8	0.161	0.247	0.464	1.363

be seen in Figs. 5, 6 and 7. The DC-bus voltage is shown in Fig. 8, and it can be seen that it is always kept constant despite the DCMG's changing working conditions.

The solar's insolation unexpectedly changes at t=2 s, causing the PV output power to drop from 10.34 kW to 7.259 kW while all other parameters stay constant. As seen in Fig. 7, the charging power of the BESS diminishes as the overall generation drops. The load demand, however, increased from 3.13 kW to 12.73 kW at t=3 s. Currently, generation falls short of the overall load demand. To maintain power balance, the BESS starts discharging its power via boost mode, as shown in Fig. 7.

On the other hand, at t=4 s, the generation from the SPV unit increases from 7.259 kW to 9.33 kW due to the improvement in atmospheric conditions. However, still, the total generation is less than the load demand. So, to maintain the power balance, the battery discharges its power through the boost mode, as shown in Fig. 7. Meanwhile, the load demand at t=7 s suddenly decreases from 12.73 kW to 3.13 kW. At this moment, the battery is charging through buck mode because total generation exceeds total load demands.

Moreover, the SPV resumes normal functioning at t = 8 s, but all other conditions are kept the same. In such a case, the battery will charge in boost mode to maintain a power balance in the MG. The power and the DC-bus voltage responses exhibit huge transients due to alteration of the MG's operating point numerous times over the simulation period, as illustrated in Figs. 5, 6, 7, and 8. However, in terms of setup time, the designed ITSMC outperforms the existing SMC in managing the DCMG's transient stability.

In addition, the performance of the designed controller is compared to that of the existing controller under various operating conditions, as stated in this section, in terms of settling time, peak value, and percentage overshoot. Tables 2, 3 4 and 5 show the settling time, peak value, and percentage overshoot for various DC microgrid components over various transient times. The designed controller, as indicated in these

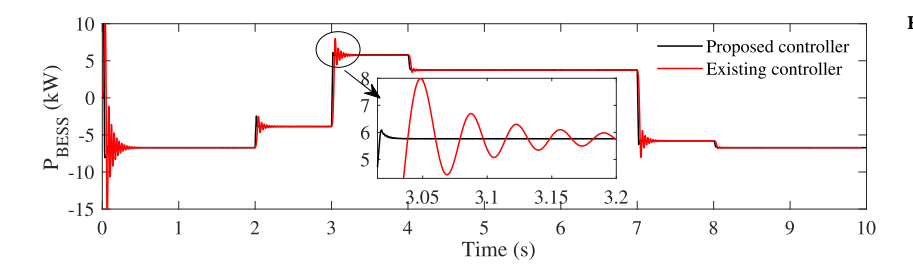


Fig. 7. BESS power response in the DC microgrid.

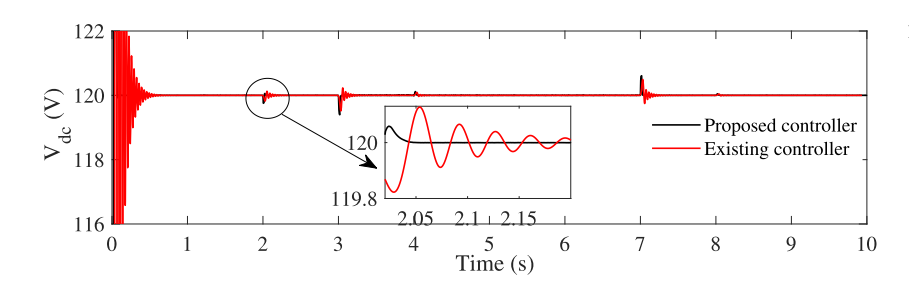


Fig. 8. DC-bus voltage response in the DC microgrid.

Table 3Quantitative evaluation for the DC load.

Transient time	Settling time (s)		Overshoot %	
(s)	Proposed	Existing	Proposed	Existing
3	0.022	0.404	0	15.813
7	0.022	0.400	0	40.095

Table 4Quantitative evaluation for the BESS.

Transient time	Settling time (s)		Overshoot %	
(s)	Proposed	Existing	Proposed	Existing
2	0.02	0.09	33.947	144.791
3	0.02	0.10	0	59.761
4	0.02	0.05	0	11.564
7	0.01	0.06	0	37.873
8	0.01	0.02	0	1.246

Table 5Quantitative evaluation for the DC-bus voltage.

Transient time	Settling time (s)		Overshoot %	
(s)	Proposed	Existing	Proposed	Existing
2	0.043	0.251	0.048	0.106
3	0.046	0.290	0	0.189
4	0.040	0.160	0	0.0191
7	0.047	0.303	0	0.145
8	0.01	0.06	0	0.873

tables, has a lower proportion of overshoots, a lower peak value, and shorter settling times than the existing controller in all operating scenarios. Therefore, according to the findings of the aforementioned analysis, it can be concluded that the designed controller outperforms the existing controller in every regard.

The following section goes over performance evaluation in the Hardware in Loop platform.

5.2. PIL validation

To further validate findings from theoretical and simulation studies, the Hardware in Loop (PIL) platform is used. On this platform, the control input is sent to a real-time processor (Rasberry Pi 3B Quad-

Core 64-bit Microprocessor Development Board) via a PIL block (as depicted in Fig. 9). The control signal produced by this processor is fed back to the MATLAB/Simulink platform to drive the switch of the converter. This means that the development board receives analog signals-the reference and actual measured signals for the converter-while the control signal is generated in a real-time environment. As illustrated in Fig. 9, the Ethernet line is used to send and receive data between the development board and MATLAB/Simulink. It is worth noting that the experiment's parameters are identical to those used in the prior simulations. Several scenarios are assessed in the following by changing the power generation of the solar PV unit and load demand.

The output of the solar PV unit is considered 10.34 kW under standard atmospheric conditions from t=0 s to t=3 s, whereas the load demand is 2.4 kW till t=4 s, as illustrated in Fig. 10(a) and (b), respectively. According to Fig. 10(a) and (b), there will be a power surplus of 7.94 kW that will be stored in BESS because its SoC is less than the maximum SoC limit. As illustrated in Fig. 10, the power balance can be achieved with both controllers, which is an indication of the dynamic stability of all power responses and the DC-bus voltage. However, when compared to the existing SMC, these responses with ITSMC exhibit superior transient characteristics.

The solar insolation unexpectedly changes at t=3 s, causing the solar PV output power to drop from 10.34 kW to 7.34 kW while all other parameters remain constant. As seen in Fig. 10(c), the charging power of the BESS declines as overall generation drops. However, at t=4 s, the load demand increased from 2.4 kW to 7.198 kW. Even if the total generation is greater than the total load demand at this moment, the BESS switches to the discharging phase of operation to maintain the power balance because of internal system power losses as shown in Fig. 10(c).

On the other hand, due to the improvement in atmospheric conditions at t = 7 s, the generation from the solar PV unit jumps from 7.34 kW to 8.821 kW. As a result, the total generation in the DCMG is greater because the overall load demand remains constant. As a result, the battery switches to the charging phase in order to preserve power balance, as depicted in Fig. 10(c).

Again, the load demand suddenly increased from 7.198 kW to 7.486 kW at t = 8 s. However, at this stage, the BESS continues to charge via buck mode since the overall generation is greater than the total load requirement. Again, at t = 9 s, the solar PV resumes its normal operation, but the load demand keeps the same. In order to preserve the power balance within the DCMG, the buck mode is kept running to charge the battery with additional power.

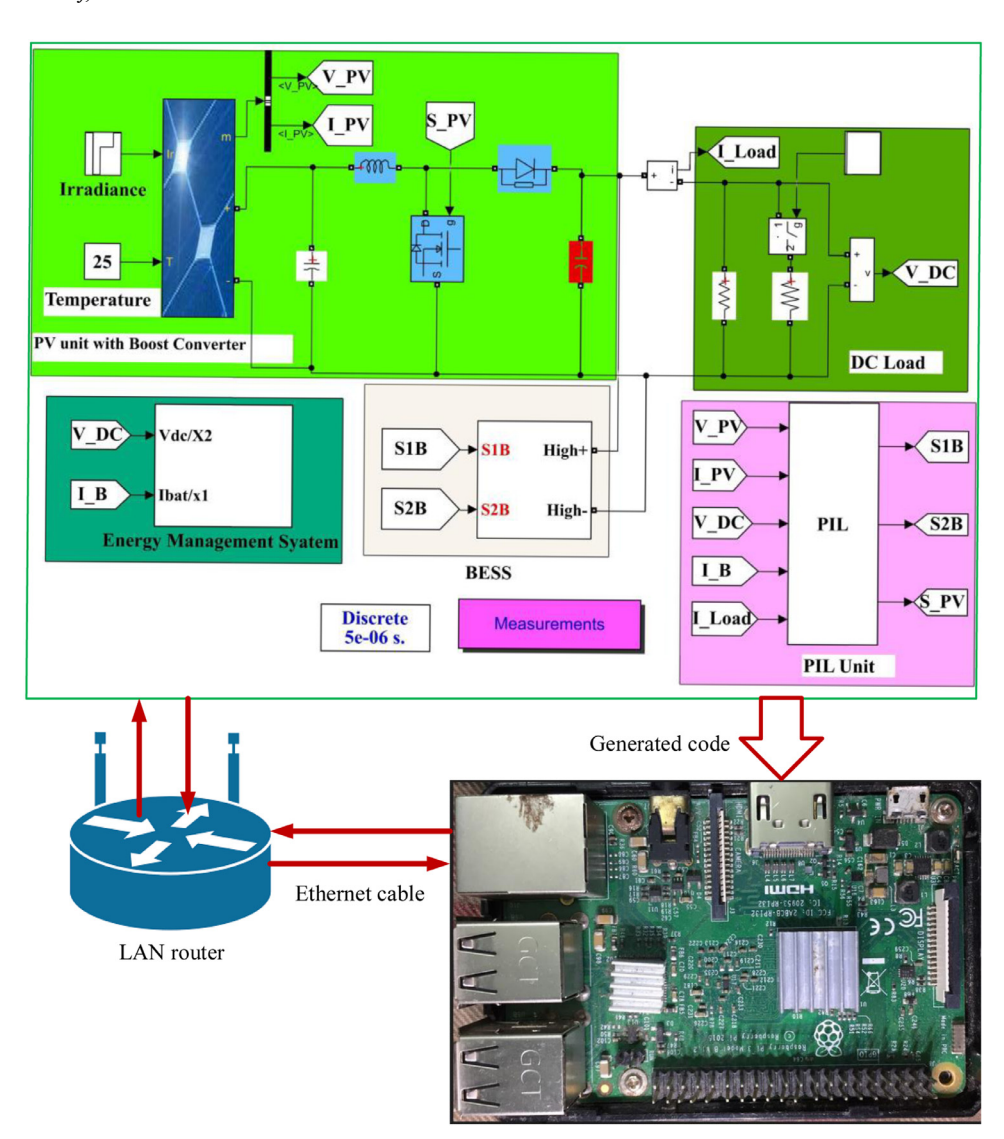


Fig. 9. The implementation of the proposed DC microgrid in Hardware in Loop platform.

From the above real-time simulation, it is obvious that the microgrid's operating point is being changed multiple times over the simulation time. There are large transients in the power responses and the DC-bus voltage responses, as shown in Fig. 10. However, in terms of overshoot and settling time, the designed ITSMC outperforms the existing SMC in managing the DCMG's transient stability.

6. Conclusion

A nonlinear double power reaching law-based integral terminal sliding mode controller is built for each component in a DCMG to adjust output power while maintaining power balance for the energy nexus. The proposed controller's theoretical analysis is presented using the control Lyapunov function. Under various conditions, such as shifting solar

irradiation and fluctuating load demand, the results are studied in both simulation and processor-in-loop platforms. Both simulation and PIL results indicate that the proposed controller is capable of achieving faster transient and dynamic stability under a variety of DCMG operation conditions. The consequences of model perturbations and external disruptions are not accounted for in the mathematical model. Therefore, future work will improve the controller design process by including these implications into the model.

Declaration of Competing Interest

The authors declare that they have no known competing financial interests or personal relationships that could have appeared to influence the work reported in this paper.

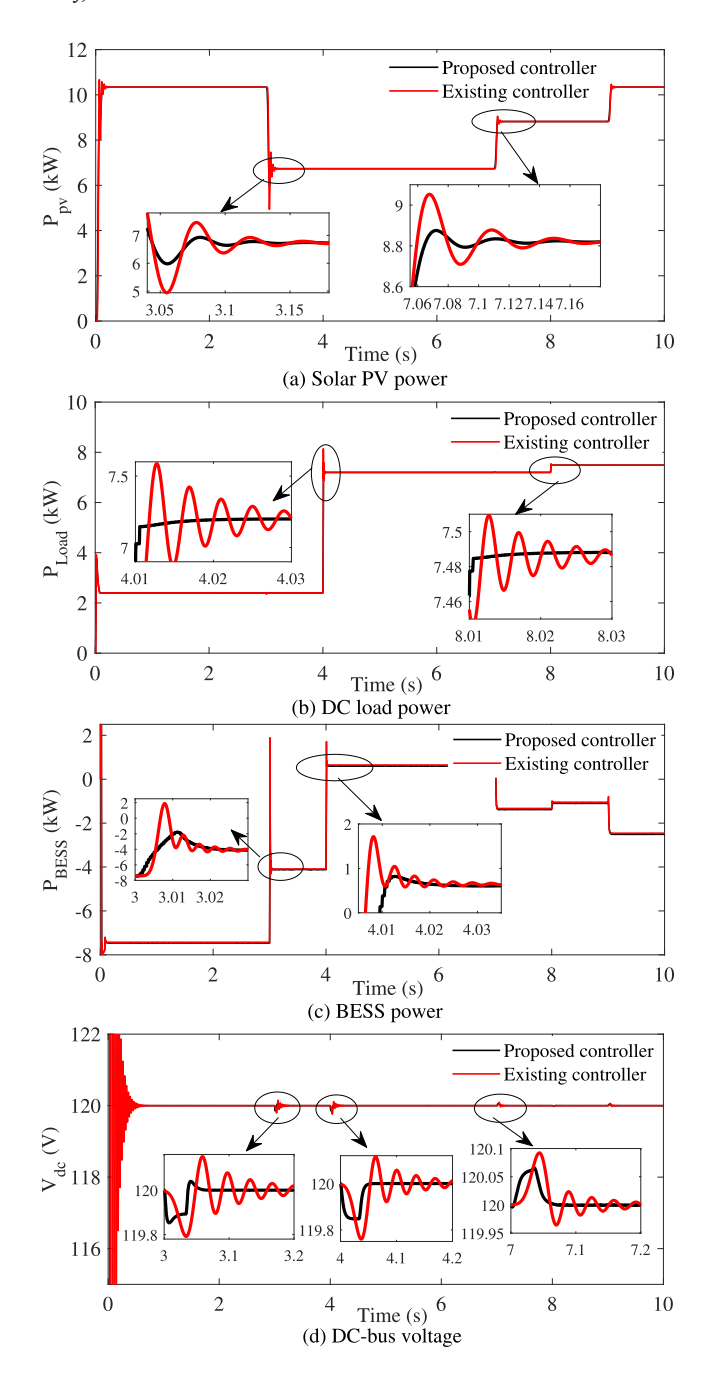


Fig. 10. Dynamic and transient stability of the solar PV unit, DC load, BESS unit, and DC-bus voltage in the hardware in loop platform.

References

- T.K. Roy, M.A. Mahmud, Active power control of three-phase grid-connected solar PV systems using a robust nonlinear adaptive backstepping approach, Solar Energy, 153 (2017) 64–76.
- [2] M.M. Rahman, E. Velayutham, Renewable and non-renewable energy consumption-economic growth nexus: new evidence from South Asia, Renew. Energy 147 (2020) 399–408.
- [3] O. Bamisile, A. Babatunde, H. Adun, N. Yimen, M. Mukhtar, Q. Huang, W. Hu, Electrification and renewable energy nexus in developing countries; an overarching analysis of hydrogen production and electric vehicles integrality in renewable energy penetration, Energy Convers. Manage. 236 (2021) 114023.
- [4] D. Nafus, E.M. Schooler, K.A. Burch, Carbon-Responsive computing: changing the nexus between energy and computing, Energies 14 (21) (2021) 6917.
- [5] R.M. Kamel, Effect of wind generation system types on micro-grid (MG) fault performance during both standalone and grid connected modes, Energy Convers. Manage., 79 (2014) 232–245.

- [6] D.E. Olivares, C.A. Cañizares, M. Kazerani, A centralized energy management system for isolated microgrids. IEEE Trans. Smart Grid 5 (4) (2014) 1864–1875.
- [7] Y.-C. Chang, C.-M. Liaw, Establishment of a switched-reluctance generator-based common DC microgrid system, IEEE Trans. Power Electron., 26 (9) (2011) 2512–2527.
- [8] Q. Jiang, M. Xue, G. Geng, Energy management of microgrid in grid-connected and stand-alone modes, IEEE Trans. Power Syst., 28 (3) (2013) 3380–3389.
- [9] T. Jin, H. Li, S.P. Kumar Prabha, Supply chain design for transactive energy operations in the nexus of manufacturing, microgrid and climate, J. Oper. Res. Soc. (2022) 1–17
- [10] Y. Pezhmani, M.Z. Oskouei, N. Rezaei, H. Mehrjerdi, A centralized stochastic optimal dispatching strategy of networked multi-carrier microgrids considering transactive energy and integrated demand response: application to water-energy nexus, Sustain. Energy Grids Netw. 31 (2022) 100751.
- [11] S. Emmanouil, J. Philhower, S. Macdonald, F.K. Khadim, M. Yang, E. Atsbeha, H. Nagireddy, N. Roach, E. Holzer, E.N. Anagnostou, A comprehensive approach to the design of a renewable energy microgrid for rural Ethiopia: the technical and social perspectives, Sustainability 13 (7) (2021) 3974.
- [12] P. Satapathy, S. Dhar, P. Dash, A mutated hybrid firefly approach to mitigate dynamic oscillations of second order PLL based PV-battery system for microgrid applications, Sustain. Energy Technol. Assess., 16 (2016) 69–83.
- [13] D. Pavković, M. Lobrović, M. Hrgetić, A. Komljenović, A design of cascade control system and adaptive load compensator for battery/ultracapacitor hybrid energy storage-based direct current microgrid, Energy Convers. Manage., 114 (2016) 154–167.
- [14] D.K. Dhaked, D. Birla, Modeling and control of a solar-thermal dish-stirling coupled PMDC generator and battery based DC microgrid in the framework of the ENERGY NEXUS, Energy Nexus 5 (2022) 100048.
- [15] H.M. Sultan, A.S. Menesy, S. Kamel, A. Korashy, S. Almohaimeed, M. Abdel-Akher, An improved artificial ecosystem optimization algorithm for optimal configuration of a hybrid PV/WT/FC energy system, Alex. Eng. J., 60 (1) (2021) 1001–1025.
- [16] C. Wang, X. Li, L. Guo, Y.W. Li, A nonlinear-disturbance-observer-based DC-bus voltage control for a hybrid AC/DC microgrid, IEEE Trans. Power Electron., 29 (11) (2014) 6162–6177.
- [17] S. Li, P. Zhao, C. Gu, J. Li, S. Cheng, M. Xu, Online battery protective energy management for energy-transportation nexus, IEEE Trans. Ind. Inf. (2022).
- [18] D.T. Abdul-hamied, A.M. Shaheen, W.A. Salem, W.I. Gabr, R.A. El-sehiemy, Equilibrium optimizer based multi dimensions operation of hybrid AC/DC grids, Alex. Eng. J., 59 (6) (2020) 4787–4803.
- [19] N. Eghtedarpour, E. Farjah, Distributed charge/discharge control of energy storages in a renewable-energy-based DC micro-grid, IET Renew. Power Gener., 8 (1) (2014) 45–57.
- [20] Y.A.-R.I. Mohamed, E.F. El-Saadany, Adaptive decentralized droop controller to preserve power sharing stability of paralleled inverters in distributed generation microgrids, IEEE Trans. Power Electron., 23 (6) (2008) 2806–2816.
- [21] M. ElMenshawy, A. Massoud, Development of modular DC-DC converters for low-Speed electric vehicles fast chargers, Alex. Eng. J., 60 (1) (2021) 1067–1083.
- [22] S. Sanchez, M. Molinas, Degree of influence of system states transition on the stability of a DC microgrid, IEEE Trans. Smart Grid, 5 (5) (2014) 2535–2542.
- [23] S.K. Ghosh, T.K. Roy, M.A.H. Pramanik, A.K. Sarkar, M. Mahmud, et al., An energy management system-based control strategy for DC microgrids with dual energy storage systems, Energies 13 (11) (2020) 2992.
- [24] L. Maharjan, T. Yamagishi, H. Akagi, Active-power control of individual converter cells for a battery energy storage system based on a multilevel cascade PWM converter, IEEE Trans. Power Electron., 27 (3) (2010) 1099–1107.
- [25] Q. Ye, R. Mo, H. Li, Low-frequency resonance suppression of a dual-active-bridge DC/DC converter enabled DC microgrid, IEEE J. Emerg. Sel. Top.Power Electron., 5 (3) (2017) 982–994.
- [26] F. Jalilian, M.A. Mirzaei, K. Zare, B. Mohammadi-Ivatloo, M. Marzband, A. Anvari-Moghaddam, Multi-energy microgrids: an optimal despatch model for water-energy nexus, Sustain. Cities Soc. 77 (2022) 103573.
- [27] E. Whitney, W.E. Schnabel, S. Aggarwal, D. Huang, R.W. Wies, J. Karenzi, H.P. Huntington, J.I. Schmidt, A.D. Dotson, MicroFEWs: a food–energy–water systems approach to renewable energy decisions in islanded microgrid communities in rural Alaska, Environ. Eng. Sci. 36 (7) (2019) 843–849.
- [28] W. Zhang, A. Valencia, L. Gu, Q.P. Zheng, N.-B. Chang, Integrating emerging and existing renewable energy technologies into a community-scale microgrid in an energy-water nexus for resilience improvement, Appl. Energy 279 (2020) 115716.
- [29] F. Moazeni, J. Khazaei, J.P.P. Mendes, Maximizing energy efficiency of islanded micro water-energy nexus using co-optimization of water demand and energy consumption, Appl. Energy 266 (2020) 114863.
- [30] N. Yang, D. Paire, F. Gao, A. Miraoui, W. Liu, Compensation of droop control using common load condition in DC microgrids to improve voltage regulation and load sharing, ., 64 (2015) 752–760.
- [31] Y.A.-R.I. Mohamed, E.F. El-Saadany, Adaptive decentralized droop controller to preserve power sharing stability of paralleled inverters in distributed generation microgrids, IEEE Trans. Power Electron., 23 (6) (2008) 2806–2816.
- [32] H. Kakigano, Y. Miura, T. Ise, Distribution voltage control for DC microgrids using fuzzy control and gain-scheduling technique, IEEE Trans. Power Electron., 28 (5) (2012) 2246–2258.
- [33] T. Vigneysh, N. Kumarappan, Autonomous operation and control of photo-voltaic/solid oxide fuel cell/battery energy storage based microgrid using fuzzy logic controller, Int. J. Hydrogen Energy, 41 (3) (2016) 1877–1891.
- [34] M.M. Mardani, M.H. Khooban, A. Masoudian, T. Dragičević, Model predictive control of DC-DC converters to mitigate the effects of pulsed power loads in naval DC microgrids, IEEE Trans. Ind. Electron., 66 (7) (2018) 5676–5685.

- [35] T. Dragičević, Dynamic stabilization of DC microgrids with predictive control of point-of-load converters, IEEE Trans. Power Electron., 33 (12) (2018) 10872–10884.
- [36] M.A. Mahmud, T.K. Roy, S.N. Islam, S. Saha, M.E. Haque, Nonlinear decentralized feedback linearizing controller design for islanded DC microgrids, Electr. Power Compon. Syst., 45 (16) (2017) 1747–1761.
- [37] M.A. Mahmud, T.K. Roy, S. Saha, M.E. Haque, H.R. Pota, Robust nonlinear adaptive feedback linearizing decentralized controller design for islanded DC microgrids, IEEE Trans. Ind. Appl., 55 (5) (2019) 5343–5352.
- [38] T. Roy, M. Pervej, F. Tumpa, L. Paul, Nonlinear adaptive controller design for velocity control of a DC motor driven by a DC-DC buck converter using backstepping approach, in: 2nd Int. Conference on Electrical, Computer & Telecommunication Engineering, 2016, pp. 1–4.
- [39] T.K. Roy, M.A. Mahmud, Dynamic stability analysis of hybrid islanded DC microgrids using a nonlinear backstepping approach, IEEE Syst. J., 12 (4) (2017) 3120–3130.
 [40] T.K. Roy, M.A. Mahmud, A.M. Oo, Operations of DC microgrids in coordination
- [40] T.K. Roy, M.A. Mahmud, A.M. Oo, Operations of DC microgrids in coordination with AC grids based on nonlinear backstepping controllers, in: IEEE Power & Energy Society General Meeting, 2018, pp. 1–5.
- [41] T.K. Roy, M.A. Mahmud, A.M.T. Oo, M.E. Haque, K.M. Muttaqi, N. Mendis, Nonlinear adaptive backstepping controller design for islanded DC microgrids, IEEE Trans. Ind. Appl., 54 (3) (2018) 2857–2873.
- [42] T.K. Roy, M.A. Mahmud, A.M.T. Oo, M.E. Haque, K.M. Muttaqi, N. Mendis, Non-linear adaptive backstepping controller design for controlling bidirectional power flow of BESSs in DC microgrids, in: 2016 IEEE Industry Applications Society Annual Meeting, 2016, pp. 1–8.
- [43] Y. Mi, H. Zhang, Y. Fu, C. Wang, P.C. Loh, P. Wang, Intelligent power sharing of DC isolated microgrid based on fuzzy sliding mode droop control, IEEE Trans. Smart Grid, 10 (3) (2018) 2396–2406.

- [44] S.K. Ghosh, T.K. Roy, M. Pramanik, A. Hanif, M. Mahmud, et al., Design of nonlinear backstepping double-integral sliding mode controllers to stabilize the DC-bus voltage for DC-DC converters feeding CPLs, Energies 14 (20) (2021) 6753.
- [45] C. Liang, Y. Zhang, X. Ji, X. Meng, Y. An, Q. Yao, DC bus voltage sliding-mode control for a DC microgrid based on linearized feedback, in: Chinese Automation Congress, 2019, pp. 5380–5384.
- [46] A. Esmaeli, Retracted: Stability analysis and control of microgrids by sliding mode control, 2016.
- [47] U.K. Kalla, B. Singh, S.S. Murthy, C. Jain, K. Kant, Adaptive sliding mode control of standalone single-phase microgrid using hydro, wind, and solar PV array-based generation, IEEE Trans. Smart Grid, 9 (6) (2017) 6806–6814.
- [48] S. Chaturvedi, D. Fulwani, J.M. Guerrero, Adaptive-SMC based output impedance shaping in DC microgrids affected by inverter loads, IEEE Trans. Sustain. Energy, 11 (4) (2020) 2940–2949.
- [49] V. Kumar, S.R. Mohanty, S. Kumar, Event trigger super twisting sliding mode control for DC micro grid with matched/unmatched disturbance observer, IEEE Trans. Smart Grid, 11 (5) (2020) 3837–3849.
- [50] S.K. Gudey, R. Gupta, Recursive fast terminal sliding mode control in voltage source inverter for a low-voltage microgrid system, IET Gener. Transm. Distrib., 10 (7) (2016) 1536–1543.
- [51] T.K. Roy, M.A. Mahmud, A. Nasiruzzaman, M.A. Barik, A.M.T. Oo, A non-singular fast terminal sliding mode control scheme for residual current compensation inverters in compensated distribution networks to mitigate powerline bushfires, IET Gener. Transm. Distrib., 15 (9) (2021) 1421–1434.
- [52] W. Gao, J.C. Hung, Variable structure control of nonlinear systems: anew approach, IEEE Trans. Ind. Electron., 40 (1) (1993) 45–55.